

The dynamic response of Jakobshavn Isbræ to calving rate perturbations

J. H. Bondzio et al.

Modelling the dynamic response of Jakobshavn Isbræ, West Greenland, to calving rate perturbations

J. H. Bondzio¹, H. Seroussi², M. Morlighem³, T. Kleiner¹, M. Rückamp¹,
A. Humbert^{1,4}, and E. Larour²

¹Alfred Wegener Institute, Helmholtz Centre for Polar and Marine Research, Bremerhaven, Germany

²Jet Propulsion Laboratory – California Institute of Technology, Pasadena, CA, USA

³Department of Earth System Science, University of California Irvine, Irvine, CA, USA

⁴University of Bremen, Bremen, Germany

Received: 14 September 2015 – Accepted: 1 October 2015 – Published: 15 October 2015

Correspondence to: J. H. Bondzio (johannes.bondzio@awi.de)

Published by Copernicus Publications on behalf of the European Geosciences Union.

Title Page

Abstract

Introduction

Conclusions

References

Tables

Figures

◀

▶

◀

▶

Back

Close

Full Screen / Esc

Printer-friendly Version

Interactive Discussion

Abstract

Calving is a major means of ice discharge of the Antarctic and Greenland Ice Sheets. The breaking off of icebergs changes the ice front configuration of marine terminating glaciers, which affects the stress regime of their upstream areas. Recent observations show the close correlation between the ice front position and the behaviour of many outlet glaciers. However, modelling of a glacier subject to calving poses various challenges. No universal calving rate parametrisation is known, and tracking of a moving ice front and the related boundary conditions in two or three spatial dimensions is non-trivial. Here, we present the theoretical and technical framework for a Level-Set Method, an implicit boundary tracking scheme, which we implemented into the Ice Sheet System Model (ISSM). The scheme allows us to study the dynamic response of a drainage basin to user-defined front ablation rates. We apply the method in a suite of experiments to Jakobshavn Isbræ, a major marine terminating outlet glacier of the western Greenland Ice Sheet. The model robustly reproduces the high sensitivity of the glacier to frontal ablation in form of calving. We find that enhanced calving is able to trigger significant acceleration of the ice stream. Upstream acceleration is sustained through a combination of various feedback mechanisms. However, lateral stress and ice influx into the trough are able to stabilise the ice stream. This study contributes to the present discussion on causes and effects of the continued changes occurring at Jakobshavn Isbræ, and emphasises that the incorporation of seasonal calving and dynamic lateral effects is key for realistic model projections of future global sea level rise on centennial time scales.

1 Introduction

Calving of icebergs is a major mean of ice discharge for marine terminating glaciers around the world. It accounts for about 50 % of the ice discharge of the Greenland and Antarctic Ice Sheets (Cuffey and Paterson, 2010; Rignot et al., 2013). Calving causes

TCD

9, 5485–5520, 2015

The dynamic response of Jakobshavn Isbræ to calving rate perturbations

J. H. Bondzio et al.

Title Page

Abstract

Introduction

Conclusions

References

Tables

Figures

◀

▶

◀

▶

Back

Close

Full Screen / Esc

Printer-friendly Version

Interactive Discussion



ice front retreat, which leads to reduced basal and lateral stress and results in upstream flow acceleration.

Understanding calving dynamics remains challenging because of the diversity of factors that can trigger calving events. Bathymetry, tides and storm swell, as well as sea ice cover and temperatures of both sea water and air are possible factors influencing calving rates. However, their effect, their respective share and their interplay seem to vary from glacier to glacier, and is not well understood. Therefore, no universal calving rate parametrisation, which can be used in macroscopic ice sheet models, exists to date (Benn et al., 2007; Cuffey and Paterson, 2010).

In order to assess the impact of calving on the dynamics of an outlet glacier, we need to implement boundary conditions at the dynamically evolving ice front. This poses a second technical challenge as the ice front position needs to be tracked, and the related boundary conditions need to be updated accordingly. Addressing these issues is rather straightforward for 1-D-flowline or 2-D-flowband models (Nick et al., 2009; Vieli and Nick, 2011), where the ice front can be tracked along the floor line. However, this type of models lacks the consistent representation of mechanisms like lateral momentum transport and ice influx of converging ice streams, which have to be parametrised instead. This parametrisation may neglect feedback effects important for simulations on decadal to centennial time scales, e.g. catchment area entrainment (Larour et al., 2012a).

Therefore, it is desirable to implement a front tracking scheme in 2-D-horizontal models, which has been addressed by a few ice sheet models only, e.g. Winkelmann et al. (2011). Various approaches to model the evolution of the shape of ice exist. Explicit methods track the position of a set of points, which represent the ice front. They require a complex technical framework to allow for geometric operations like folding and intersection of the continuum boundary, tracking singularities in curvature, and determining the position of a point in space relative to the modelled continuum. On the other hand, a suite of implicit boundary tracking methods exists, e.g. the Level-Set Method (LSM) by Osher and Sethian (1988). The LSM represents the continuum boundary

The dynamic response of Jakobshavn Isbræ to calving rate perturbations

J. H. Bondzio et al.

Title Page

Abstract	Introduction
Conclusions	References
Tables	Figures

◀ | ▶

◀ | ▶

Back	Close
------	-------

Full Screen / Esc

Printer-friendly Version

Interactive Discussion



The dynamic response of Jakobshavn Isbræ to calving rate perturbations

J. H. Bondzio et al.

Title Page

Abstract

Introduction

Conclusions

References

Tables

Figures

◀

▶

◀

▶

Back

Close

Full Screen / Esc

Printer-friendly Version

Interactive Discussion

implicitly by a contour, or “level-set”, of a scalar valued “Level-Set Function” (LSF). It easily handles topological changes of the modelled continuum, like splitting and merging of its parts. It is well suited for the use in a parallel architecture, since it is based on a partial differential equation. This allows for application to large scale ice sheet simulations. The method is well established in Continuum Fluid Mechanics (Chang et al., 1996; Groß et al., 2006), and can be used with various numerical schemes, like the Finite Differences Method or the Finite Element Method (FEM). A LSM has been applied to ice modelling in test cases (Pralong and Funk, 2004), but not to real ice sheets yet.

Jakobshavn Isbræ is a major marine terminating glacier in West Greenland, which drains about 6.5 % of the Greenland Ice Sheet (Zwally et al., 2011). It is characterised by two tributaries, which today terminate into an ice-choked fjord of about 30 km length (Figs. 1 and 2). The southern tributary exhibits high flow velocities, which are confined to a narrow, deep trough of about 5 km width. The trough retrogradely slopes inland to a maximum depth of about 1700 m below sea level (Gogineni et al., 2014). It discharges most of the ice of the drainage basin (Rignot and Mouginot, 2012). Observations have shown that the fast flowing areas of Jakobshavn Isbræ exhibit a weak bed with a considerable layer of temperate, soft ice (Lüthi et al., 2002). Most of these areas’ horizontal motion is due to basal sliding and shear in this layer. A large fraction of the ice stream’s momentum has to be transferred to the adjacent ice sheet by lateral stress. It is thus well justified to use the two-dimensional shelfy-stream approximation (SSA, MacAyeal, 1989) for model simulations of this glacier.

The basal topography of Jakobshavn Isbræ and its velocity field permit to roughly partition the catchment area into the confined, deep and fast-flowing troughs (“ice stream”) and the surrounding parts of low velocity flow (“ice sheet”). Those areas are separated by pronounced shear margins to either side of the ice stream.

Until the late 1990s, the glacier had a substantial floating ice tongue, which extended well into the ice fjord, and was fed by both tributaries. The position of the ice front remained fairly constant over time since the 1960s, and the glacier exhibited negligible seasonal variations in flow speed (Echelmeyer and Harrison, 1990). The glacier started

The dynamic response of Jakobshavn Isbræ to calving rate perturbations

J. H. Bondzio et al.

Title Page

Abstract

Introduction

Conclusions

References

Tables

Figures

◀

▶

◀

▶

Back

Close

Full Screen / Esc

Printer-friendly Version

Interactive Discussion



an ongoing phase of acceleration, thinning and retreat, that followed the breakup of its ice tongue. Seasonal variations in ice front position and flow velocity increased sharply (Joughin et al., 2004, 2008). The glacier is currently far from equilibrium, making it one of the fastest ice streams in the world and a major contributor to global sea level rise (Howat et al., 2011; Joughin et al., 2014). Observations confirm that the current ice stream dynamics are mainly controlled by the position of the ice front (Podrasky et al., 2012; Rosenau et al., 2013; Moon et al., 2014).

Various hypotheses have been proposed to explain the mechanisms behind the change. All identify the breakup of the floating ice tongue as the initial triggering mechanism of this dramatic chain of events, but different possible mechanisms have been proposed to explain the sustained acceleration, thinning and retreat of the glacier. Studies by Joughin et al. (2012) and Habermann et al. (2013) propose loss of buttressing and changes in basal conditions as the main cause behind the ongoing acceleration. On the other hand, van der Veen et al. (2011) argue that the acceleration has to be accompanied by significant weakening of the lateral shear margins. Various modelling studies of the glacier, which use 1-D-flowline and 2-D-flowband models, project unstable retreat of the glacier along its southern trough for up to 60 km inland within the next century (Vieli and Nick, 2011; Joughin et al., 2012; Nick et al., 2013). Other modelling studies argue that this type of ice stream displays stable behaviour as long as it is being fed by the surrounding ice sheet (Truffer and Echelmeyer, 2003). However, numerical modelling efforts of Jakobshavn Isbræ in the horizontal plane so far lacked the representation of a dynamically evolving ice front. Hence, the hypotheses could not be tested in a satisfactory manner.

We present here a theoretical and technical framework for a LSM used to model the dynamic evolution of an ice front. This method tracks the ice front related boundary conditions and is a step towards a more physical representation of ice front dynamics in 2-D and 3-D ice sheet models. We implemented the method into the Ice Sheet System Model (ISSM, Larour et al., 2012b), a parallel, state-of-the-art FEM ice sheet model, and apply it here to Jakobshavn Isbræ in order to model the dynamic response to

perturbations in calving rate and conclude on its sensitivity to ice front retreat over the next 120 years.

2 Theory

2.1 Ice flow model

5 We employ the SSA on both floating and grounded ice. It neglects all vertical shearing but includes membrane stresses. The ice viscosity μ follows Glen's flow law (Glen, 1958):

$$2\mu = B\dot{\epsilon}_e^{\frac{1-n}{n}}. \quad (1)$$

10 Here, $n = 3$ is Glen's flow law coefficient, B the ice viscosity parameter, and $\dot{\epsilon}_e$ the effective strain rate. We apply a Neumann stress boundary condition at the ice–air and ice–water interface, corresponding to zero air pressure and hydrostatic water pressure, respectively. A linear friction law links basal shear stress σ_b to basal sliding velocity \mathbf{v}_b on grounded ice:

$$\sigma_b = -\alpha^2 N \mathbf{v}_b, \quad (2)$$

15 where α denotes the basal friction parameter. We calculate effective basal pressure N assuming that sea water pressure applies everywhere at the glacier base. The ice thickness H evolves according to the mass transport equation:

$$\frac{\partial H}{\partial t} = -\nabla \cdot (H\mathbf{v}) + a_s + a_b. \quad (3)$$

20 Here, \mathbf{v} is the depth-averaged horizontal ice velocity, and a_s and a_b are surface and basal mass balance, respectively. We determine the grounding line position using hydrostatic equilibrium, and treat it with a sub-element parametrisation (Seroussi et al.,

2014). We refer the reader to Greve and Blatter (2009), Cuffey and Paterson (2010) and Larour et al. (2012b), respectively, for further details on ice flow modelling and its implementation in ISSM.

2.2 Level-Set Method

5 Let Ω be a computational domain in two- or three-dimensional space, and φ a real, differentiable function on $\Omega \times [0, \infty)$. We use φ to partition Ω at time t into three disjoint subdomains $\Omega_i(t)$, its complement $\Omega_c(t)$, and their common boundary $\Gamma(t)$. We omit the time dependence of these sets in the following, unless stated otherwise. Let \mathbf{x} be a point in Ω . If $\varphi(\mathbf{x}, t) < 0$, then \mathbf{x} belongs to Ω_i . If $\varphi(\mathbf{x}, t) = 0$, then \mathbf{x} lies on Γ . If
 10 $\varphi(\mathbf{x}, t) > 0$, then \mathbf{x} belongs to Ω_c . By construction, Γ , the 0-contour or “0-level-set” of φ , separates Ω_i and Ω_c .

A particle at the boundary Γ moves with the boundary speed \mathbf{w} . This motivates the “Level-Set Equation” (LSE):

$$\frac{\partial \varphi}{\partial t} + \mathbf{w} \cdot \nabla \varphi = 0. \quad (4)$$

15 This Hamilton–Jacobi type partial differential equation describes the transport of the ice boundary across Ω . We need to provide an initial field $\varphi_0(\mathbf{x}) = \varphi(\mathbf{x}, t = 0)$ on Ω to solve Eq. (4). We can propagate the unit surface normal \mathbf{n} on Γ onto Ω using the LSF by

$$\mathbf{n} = \frac{\nabla \varphi}{|\nabla \varphi|}. \quad (5)$$

20 By definition, \mathbf{n} always points into Ω_c . For more details on the Level-Set Method and its applications, we refer to Osher and Sethian (1988) and Sethian (2001).

The boundary of an ice sheet evolves with a velocity, which is the sum of the ice velocity and an ablation velocity $\mathbf{a} = -a^\perp \mathbf{n}$. The ablation rate $a^\perp = -\mathbf{a} \cdot \mathbf{n}$ is non-negative

in compliance with current glaciology terminology, and is the difference between ice boundary velocity \mathbf{w} and ice velocity \mathbf{v} projected along \mathbf{n}

$$a^\perp = (\mathbf{v} - \mathbf{w}) \cdot \mathbf{n}. \quad (6)$$

It follows that the ice boundary is stationary ($\mathbf{w} \cdot \mathbf{n} = 0$) if and only if $a^\perp = \mathbf{v} \cdot \mathbf{n}$, i.e. the ablation rate matches the ice velocity perpendicular to the ice boundary. The ablation rate a^\perp can be an input taken from observations or a suitable parametrisation.

Note that no limitations have been made with respect to the dimension of the problem in this section. Accordingly, the method could be applied to model the evolution of the glacier thickness and lateral extent simultaneously (Pralong and Funk, 2004). However, here we use the LSM to model only the horizontal extent of the ice sheet. Its vertical extent is described by the mass transport equation (Eq. 3). We assume in the remainder of the article that lateral ablation occurs in the form of calving with a calving velocity $\mathbf{c} = -c^\perp \mathbf{n}$, and that calving itself is a quasi-continuous process, consisting of frequent, but small calving events. With Eqs. (5) and (6), Eq. (4) becomes

$$\frac{\partial \varphi}{\partial t} + \mathbf{v} \cdot \nabla \varphi = c^\perp |\nabla \varphi|, \quad (7)$$

which is also known as “Kinematic Calving Front Condition” (KCFC, Greve and Blatter, 2009). The calving rate needs to be provided as a 2-D field on Ω , that can also vary with time. An example of a calving rate field can be seen in Fig. 4. The ice front Γ is advected at any time with the sum of the horizontal ice velocity and local calving rate values at the current ice front position (Fig. 3). We define the “calving flux” to be the ice volume calving at the ice front per unit time:

$$Q_{cf} = \int_{\Gamma} c^\perp(r) H(r) dr. \quad (8)$$

Calving rate and velocity need to be given on the entire computational domain Ω in order to solve the KCFC. Since field variables like velocity and thickness are only

The dynamic response of Jakobshavn Isbræ to calving rate perturbations

J. H. Bondzio et al.

Title Page	
Abstract	Introduction
Conclusions	References
Tables	Figures
◀	▶
◀	▶
Back	Close
Full Screen / Esc	
Printer-friendly Version	
Interactive Discussion	



intersecting hyperplane. Currently, ISSM is not capable of resolving those submesh scale processes.

Therefore, we opt to either fully activate or deactivate an element at every time step. Only active elements are considered for the numerical discretisation of the respective field equations. We activate a mesh element if at least one of its vertices is in Ω_i or Γ . Then we consider the entire element to consist of ice. We flag the element as ice free if it lies entirely inside Ω_c , and it is deactivated at this time step. As a consequence, the numerical ice front Γ^h runs along mesh edges, and updates of Γ^h occur in a discontinuous manner. We apply the stress boundary condition along Γ^h for numerical consistency. The strongly viscous ice rheology efficiently dampens effects of these discrete boundary condition updates. Ice front normals on Γ and Γ^h may differ significantly in direction. However, stress components tangential to \mathbf{n} cancel out along Γ^h , so that the integrated stress exerted at the ice front is close to the one applied along Γ . For all further calculations where a normal is involved, like extrapolation, the normal to the LSF (Eq. 5) is used.

The ice domain Ω_i is by definition a subset of the numerical ice domain Ω_i^h . Γ^h is thus displaced further downstream than Γ . This may lead to slightly higher resistive lateral stress at the ice front, whose magnitude depends on the excess ice area of the intersected front element and the front geometry. We choose a fine mesh resolution in the vicinity of the ice front to limit this effect.

We extrapolate the ice front thickness onto the ice-free vertices of the front elements using Eq. (9). This yields realistic ice thickness and ice thickness gradients across the front elements, that would otherwise lead to overestimated driving stress and underestimated water pressure at the ice–ocean interface. If not corrected, those two effects unrealistically increase ice velocities at the ice front, which then feed back into the mass transport and LSM schemes.

We present an idealized test-setup for validation of the LSM-module in Appendix A. It shows that the ice margin is advected with correct speed. A small error is due to the underlying unstructured mesh used, but cancels out over time. The module re-

TCD

9, 5485–5520, 2015

The dynamic response of Jakobshavn Isbræ to calving rate perturbations

J. H. Bondzio et al.

Title Page

Abstract

Introduction

Conclusions

References

Tables

Figures

◀

▶

◀

▶

Back

Close

Full Screen / Esc

Printer-friendly Version

Interactive Discussion



The dynamic response of Jakobshavn Isbræ to calving rate perturbations

J. H. Bondzio et al.

Title Page

Abstract

Introduction

Conclusions

References

Tables

Figures

◀

▶

◀

▶

Back

Close

Full Screen / Esc

Printer-friendly Version

Interactive Discussion



quires additional computational effort for the extrapolation of field variables, to solve the KCFC, and for extra iterations of the momentum balance solver, since the stress boundary condition at the ice front does often change. Its amount depends on the flow approximation used and especially on whether the model setup is close to a stable configuration or not. Using the SSA approximation, the additional computational cost amounts to up to 25 %, of which 11 % is caused by the solution of the LSM-module for this experiment.

3 Data and model setup

3.1 Jakobshavn Isbræ model setup

We use Jakobshavn Isbræ's drainage basin from Zwally et al. (2011) to generate a 2-D-horizontal finite element mesh with element size varying from 500 m in the fjord and areas of fast flow to 10 km inland (Fig. 4). We choose this high mesh resolution to minimise ice front discretisation errors, and to resolve the fjord and the deep trough accurately in the model. The resulting mesh has about 10 000 vertices and 19 000 elements. Due to high flow velocities, the numerical Courant–Friedrich–Lewy condition (Courant et al., 1928) dictates a time step length on the order of days.

We use ice bedrock topography from Morlighem et al. (2014), derived using a mass conservation approach (Morlighem et al., 2011). The ice surface elevation is taken from GIMP (Howat et al., 2014). Ice thickness is the difference between ice surface and ice base elevation. Bathymetry of the ice-choked fjord of Jakobshavn Isbræ is difficult to measure and currently poorly known. As a first order estimate, we apply a parabolic profile of 800 m depth along the ice fjord, fitted via spline interpolation to known topography data. We rely on Ettema et al. (2009) to force the surface mass balance. Their surface temperatures are used to calculate the ice viscosity parameter B following an Arrhenius relationship (Cuffey and Paterson, 2010) once at the beginning

The dynamic response of Jakobshavn Isbræ to calving rate perturbations

J. H. Bondzio et al.

Title Page

Abstract

Introduction

Conclusions

References

Tables

Figures

◀

▶

◀

▶

Back

Close

Full Screen / Esc

Printer-friendly Version

Interactive Discussion



relaxation run, continued onto Ω_c (Fig. 4). l is a continuous function, which is 1 in areas where the bedrock lies below -300 m, and linearly drops to 0 in areas of positive bedrock elevation. It prevents calving onto areas with a glacier bed above sea level, motivated by observations from tidewater glaciers (Brown et al., 1982). We expect this calving rate to yield a stationary ice front, if applied to a geometry in steady state. We scale c_0^\perp over time with a scaling function $s = s(t)$, which allows for the representation of seasonal calving cycles, and a perturbation function $p = p(t)$ to modify the calving rate for some period of time, respectively. The applied calving rate then is $c^\perp = c^\perp(\mathbf{x}, t) = c_0^\perp(\mathbf{x}) \cdot s(t) \cdot p(t)$.

We perform three suites of experiments in order to analyse the impact of the calving rate on the glacier's dynamics. The ice front is now allowed to freely evolve in response to c^\perp . All experiments run for a total time of 120 years.

In experiment A, we keep calving constant over time, i.e. we let both $s(t) = p(t) = 1$. Hence, $c^\perp(\mathbf{x}, t) = c_0^\perp(\mathbf{x})$. This experiment, although not physically motivated, is used to evaluate whether a stable ice front position can be reached using the LSM.

In experiment suites B and C, we mimic seasonal calving by scaling c_0^\perp over time by a factor $s(t) = \max(0, \pi \sin(2\pi(t/L - \phi_0)))$, with phase shift $\phi_0 = 4/12$ and period $L = 1$ a. We perturb the calving cycle during a limited perturbation duration Δt with a perturbation strength $p_0 \geq 0$:

$$p(t) = \begin{cases} p_0, & \text{if } t_0 < t < t_0 + \Delta t, \text{ and} \\ 1, & \text{else} \end{cases}$$

We start the perturbation at $t_0 = 20$ a for all experiments. In experiment suite B we choose $\Delta t = 1$ a and vary p_0 in steps of 1 from 0 to 4. On the other hand, in experiment suite C we keep $p_0 = 2$ fixed, and choose Δt as 2, 4 and 8 years. We use the notation $B < p_0 >$ and $C < \Delta t >$ to identify the single experiments, e.g. B2 for experiment B with perturbation strength $p_0 = 2$. Experiment B1 represents in this experiment suite the case of unperturbed periodic calving. It is used as a control run the other experiments

can be compared to. We introduce $P = (1 - p_0) \cdot \Delta t$, which is a measure of the time-integrated deviation in applied calving rate relative to B1.

4 Results

We present ice front positions for several experiments in Fig. 5. Under constant calving rate forcing, the ice front essentially remains at a stable position after minor readjustments in the first decade of the simulation. In experiment A, the ice front undergoes gradual retreat over time. When we perturb the calving rate, the ice front migrates. Increased calving rates cause ice front retreat: higher calving rates lead to larger retreats. The retreat is highest in areas of fast ice flow, but strongly decreases towards the ice stream margins. This yields the characteristic concave shape of a retreating ice front. Resulting ice fronts positions and their characteristics do agree well with ice fronts obtained from observations (Fig. 2). Ice front positions of all experiments B and C readvance after the perturbation interval to a position which is indistinguishable from the one of B1 in one to two decades.

Figure 6 shows ice velocity, geometry and strain rates along two tracks, which go along and across the southern trough, respectively (Fig. 4). We observe that the ice front position, its ice velocity and thickness as well as the position of the grounding line form an ensemble, which quickly adjust to each other under constant mean annual calving rates to reach a characteristic “ice front configuration”. The variables of the ice front configuration mirror the minor adjustment of the ice front position prior to the perturbation. Only the ice thickness in the floating part decreases up to 100 m once the ice front is allowed to freely adjust. Enhanced calving causes the modelled ice stream to rapidly thin, accelerate and retreat. However, the ice front can be very thick at the end of the calving season, as the glacier has retreated back into areas of high ice thickness. Ice velocities respond to this change by increasing over time as the ice front retreats and peaking at the point of furthest retreat. The response is stronger with larger and longer perturbations, as expected. The acceleration of the ice stream extends well up-

TCD

9, 5485–5520, 2015

The dynamic response of Jakobshavn Isbræ to calving rate perturbations

J. H. Bondzio et al.

Title Page

Abstract

Introduction

Conclusions

References

Tables

Figures

◀

▶

◀

▶

Back

Close

Full Screen / Esc

Printer-friendly Version

Interactive Discussion



stream to areas of grounded ice. Both thinning and acceleration mainly occur in the ice stream itself, and diffuse out to the surrounding ice sheet in a strongly dampened fashion. These thinning and acceleration patterns increase surface and velocity gradients along and across the ice stream, especially in the shear margins. Here, the ice stream acceleration gradually increases effective strain rates up to a factor of 4 in experiment C4, which corresponds to a drop in viscosity of 60 % (Eq. 1). This weakens the mechanical coupling between the ice stream and the surrounding ice sheet substantially. The grounding line position lies downstream of a local high of the basal topography at any given time of the experiment, even if the general slope of the basal topography is retrograde. It is hardly affected by small calving rate perturbations. However, large perturbations cause discontinuous migration of its position to the next topographic high upstream. Their discrete locations form the set of stable grounding line positions along the deep part of the tributaries. Discontinuous retreat of the grounding line causes drastic, but short-lived flow acceleration, which indicates that the basal topographic highs act as pinning points, even if basal friction coefficient α and effective basal pressure N in the troughs are low.

Timelines of ice front position, ice velocity and thickness at the ice front, as well as effective strain rate and position of the first grounded point along-trough are shown in Fig. 7. They allow us to study the interannual behaviour of the ice front configuration in more detail. All shown variables reflect the characteristics of the applied calving rate forcing. They stay constant in experiment A, and oscillate periodically with a constant amplitude around an annual mean value in experiment suites B and C.

Prior to the perturbation, the ice front position varies by ± 3 km along-stream. Ice velocities and front thickness act in phase to the ice front position, while the response of strain rates at the grounding line is slightly delayed. Ice velocities vary by $\pm 20\%$, which corresponds to about $\pm 2 \text{ km a}^{-1}$, ice thickness by $\pm 13\%$, or ± 100 m, and effective grounding line strain rates by $\pm 7\%$, or $\pm 0.1 \text{ a}^{-1}$. The grounding line position is stable at kilometre 29 of the along-trough profile. In response to a two-fold increase in calving rate, the ice front retreats initially at an average rate of 4.5 km a^{-1} (Fig. 7d).

The dynamic response of Jakobshavn Isbræ to calving rate perturbations

J. H. Bondzio et al.

Title Page

Abstract

Introduction

Conclusions

References

Tables

Figures

◀

▶

◀

▶

Back

Close

Full Screen / Esc

Printer-friendly Version

Interactive Discussion



The dynamic response of Jakobshavn Isbræ to calving rate perturbations

J. H. Bondzio et al.

Title Page

Abstract

Introduction

Conclusions

References

Tables

Figures

◀

▶

◀

▶

Back

Close

Full Screen / Esc

Printer-friendly Version

Interactive Discussion

This retreat rate decreases to zero for longer perturbations, so that the ice front approaches a new stable position upstream. Variation of the ice front position during the retreat doubles to up to ± 6.5 km. Average ice velocity increases by about 10 %, but its variation also almost doubles to ± 38 %. Occasional velocity spikes occur related to ungrounding from pinning points. The ice front thins on average by a third, with oscillations up to ± 75 %. This high thickness variation is due to the calving back into areas of thick ice in summer followed by stretching and thinning during ice front advance in the late winter season. Variation of the grounding line position remains small during the perturbation, disrupted only by its discontinuous retreat for large perturbations. For small perturbations (Fig. 7c), variation of effective strain rates here quadruples to ± 25 %. Once the calving rate perturbation ceases, the ice front configuration displays a striking reversibility in all its variables.

Finally, Fig. 8 shows the evolution of the total ice volume as modelled against control run B1. The mean annual volume change due to ongoing geometry relaxation of experiment B1 is $-22.8 \text{ km}^3 \text{ a}^{-1}$, varying by $\pm 10.5 \text{ km}^3$ per year. Experiment A undercuts this value by $-0.4 \text{ km}^3 \text{ a}^{-1}$ on average related to the gradual retreat of its ice front. Enhanced calving causes additional volume loss proportional to perturbation measure P . It amounts to $-35.7 \text{ km}^3 \text{ a}^{-1}$ in the first year of perturbation of experiment C8, but decreases with time, as the ice front thins and retreats into areas of lower calving rates. Those numbers agree well with recent ice discharge observations (Howat et al., 2011). After the perturbation, all modelled glaciers recover 40–60 % of the volume difference in the first decade, because during the readvance the thin ice front strongly reduces the calving flux. The calving flux converges to the value of experiment B1 once the ice front configuration approaches the state of the control run. The ice volume now has to be replenished by excess surface accumulation, which takes longer than the 120 years of simulation time presented here. Calving rate perturbations therefore leave a lasting imprint on the ice sheet.

Results of experiments of decreased calving are not shown here. They exhibit the exact inverse pattern to the one described above for enhanced calving: the ice front

advances during the perturbation, creating a convex ice tongue. Meanwhile, the ice stream decelerates and thickens, causing grounding line advance and volume increase. After the perturbation period, the glacier calves back into a state slightly thicker and faster than the one of B1.

5 Discussion

The characteristics of the applied calving rate determine the behaviour of the ice front. The ice front will reach a stable configuration if the calving rate exceeds the ice velocity from some point along-stream onward. It will either retreat back or advance to this point. If no such point exists, the ice front will undergo either unconfined advance or retreat, depending on the magnitude of the calving rate.

Adjustments of the ice front configuration to the current calving rate change the local driving stress, which lead to corresponding changes in thickness and surface gradient, and vice versa. The mass transport mechanism allows the thickness change to diffuse upstream. In case of ice front thinning and surface steepening, the increased driving stress leads to enhanced mass flux, causing further upstream thinning, steepening and acceleration.

We observe multiple secondary feedback mechanisms in addition to the mass transport mechanism, that determine the way the ice sheet adjusts to calving rate forcings. Thinning of the ice stream leads to reduced basal effective pressure and grounding line retreat, which both reduce basal drag significantly. Detachment of the base from pinning points leads to short-lived, but drastic increases in ice flux. These mechanisms are qualitatively the same as the ones described in Vieli and Nick (2011) and Joughin et al. (2012).

The ice front lengthens during its retreat, which increases the total driving stress exerted by the ice front. Side arms of the main tributaries are now calving directly into the fjord. This increases calving flux Q_{cf} , which additionally thins and steepens areas in the immediate ice front vicinity.

The dynamic response of Jakobshavn Isbræ to calving rate perturbations

J. H. Bondzio et al.

Title Page

Abstract

Introduction

Conclusions

References

Tables

Figures

◀

▶

◀

▶

Back

Close

Full Screen / Esc

Printer-friendly Version

Interactive Discussion



The dynamic response of Jakobshavn Isbræ to calving rate perturbations

J. H. Bondzio et al.

Title Page

Abstract

Introduction

Conclusions

References

Tables

Figures

◀

▶

◀

▶

Back

Close

Full Screen / Esc

Printer-friendly Version

Interactive Discussion

The steepening of the surface slopes across the shear margins caused by ice stream thinning results in increased driving stress, which increases lateral ice inflow into the ice stream. This in turn limits surface steepening and grounding line retreat along the trough. The feedbacks described above cause a net rise in volume flux towards the ice front and enable quick adjustment of the glacier in response to changes of the ice front configuration.

Acceleration of the ice stream and surface steepening in its vicinity strongly increase strain rates at the shear margins and the grounding line. The non-linear rheology of ice softens these areas, allowing the ice stream to accelerate further, and to soften its shear margins more and more. This positive feedback is only controlled by the rate at which ice is able to enter the ice stream to sustain the driving stress. We consider this mechanism to be substantial for sustaining the longer term ice stream acceleration, since a large fraction of the ice stream's driving stress is balanced by lateral stress. This corroborates force balance arguments produced earlier by van der Veen et al. (2011).

Reduced lateral momentum transfer decreases lateral mass influx. This makes the surrounding ice sheet less sensitive to short periods of enhanced calving. For this reason, calving induced thinning mainly occurs in the ice stream, which limits the rate at which additional ice can be discharged.

Conversely, in case of no seasonal calving cycle of experiment A, mechanical coupling between the ice stream and ice sheet is higher than compared to experiment B1. Ice stream velocity is therefore lower, which causes net ice front retreat and corresponding volume loss. This illustrates that ice sheet models which do not include a seasonal calving cycle may overestimate mass loss of glaciers. Moreover, we do advise against the use of ice models, which do not incorporate a dynamically evolving ice front nor the related lateral effects, for projections of future contributions to global sea level rise on decadal to centennial time scales.

Response mechanisms not covered here will likely include feedbacks in damage mechanics and thermodynamics due to the increased strain rates. During longer per-

turbations, ice surface lowering will probably affect the surface mass balance and the drainage basin outline.

The reversibility of the ice front configuration after the calving rate perturbation is a robust feature across all experiments. We see the short duration of the perturbation, the prescribed calving rates and the geometric setting of the ice stream to be responsible for this behaviour. Volume change relative to experiment B1 is mainly due to the migration of the ice front and the according change in lateral ice sheet extent. However, the additional ice discharge never exceeds 0.1 % of the total glacier volume in the experiments shown here. This volume loss can be easily balanced by the vast surrounding ice sheet. Since calving rates are not coupled to ice dynamics, the ice front configuration is able to quickly recover once this forcing is set back to its initial value.

The modelled glacier response due to enhanced calving is in good agreement with observations. However, the reversibility of the ice front position is in stark contrast to Jakobshavn Isbræ's ongoing observed retreat. Therefore, the actual calving rates must have stayed increased, as our results suggest that the glacier would have readvanced otherwise.

6 Conclusions

We presented the theoretical framework for coupling a LSM to ice dynamics and implemented it into the ISSM. The LSM proved to be a robust method for modelling the dynamic evolution of an ice front subject to ablation. We applied the technique to Jakobshavn Isbræ using prescribed calving rates. We find its dynamics to be highly sensitive to the applied calving rate, which agrees well with observations.

The calving rate perturbation strongly affects the ice flow inland through various mechanisms. Changes in calving rate cause ice front migration and alter its ice discharge. The resulting thickness change at the ice front diffuses upstream through a coupling between the stress balance and mass transport mechanism. Ice stream thinning reduces basal drag by means of grounding line retreat and reduction of effective

The dynamic response of Jakobshavn Isbræ to calving rate perturbations

J. H. Bondzio et al.

Title Page

Abstract

Introduction

Conclusions

References

Tables

Figures

◀

▶

◀

▶

Back

Close

Full Screen / Esc

Printer-friendly Version

Interactive Discussion



The dynamic response of Jakobshavn Isbræ to calving rate perturbations

J. H. Bondzio et al.

Title Page

Abstract

Introduction

Conclusions

References

Tables

Figures

◀

▶

◀

▶

Back

Close

Full Screen / Esc

Printer-friendly Version

Interactive Discussion



basal pressure. Rheological shear margin weakening caused by ice stream acceleration decreases lateral drag resistive to flow. These two positive feedback mechanisms are able to sustain prolonged acceleration of the ice stream, and are only controlled by the rate at which ice can enter the ice stream. However, the vast surrounding ice sheet is barely affected by short periods of enhanced calving. It stabilises the ice stream and allows for quick reversibility of the ice front configuration through lateral mass influx and stress transfer once we set the calving rates back to their initial value. The importance of the ice front position and lateral effects for the behaviour of this type of glacier lets us advise against the use of models, which do not represent these mechanisms, for projections of future ice discharge.

The method presented here is able to close a major gap present in ISSM and various other ice sheet models. It enables a multitude of future studies in combination with e.g. thermodynamics and damage mechanics, and will improve our understanding of outlet glaciers.

Appendix: Test-setup

We present a simple test setup to validate the LSM. Let Ω be a 50 km square with an initial LSF as

$$\varphi_0(\mathbf{x}) = \|\mathbf{x} - \mathbf{x}_0\|_2 - R,$$

where $\mathbf{x}_0 = (25, 25)$ km and $R = 12.5$ km, so that our initial 0-level-set describes a circle in the middle of the domain. We prescribe a constant velocity of $\mathbf{v} = 1 \text{ km a}^{-1} \cdot (\cos(\pi/4), \sin(\pi/4))$ everywhere. We advect φ_0 over 10 years with time steps of 0.1 a, and keep track of its 0-level-set.

We plot the 0-level-set position at the beginning every year in Fig. A1. The initial circular shape is preserved and advected with constant speed. We measure the advection speed of the 0-level-set along the diagonal marked in white in Fig. A1. Figure A2 shows the standard deviation of its numerical error relative to the prescribed advection speed

The dynamic response of Jakobshavn Isbræ to calving rate perturbations

J. H. Bondzio et al.

Title Page

Abstract

Introduction

Conclusions

References

Tables

Figures

◀

▶

◀

▶

Back

Close

Full Screen / Esc

Printer-friendly Version

Interactive Discussion



for different element sizes. The numerical error is mainly related to the interpolated representation of the curved shape on an irregular mesh. This causes the front velocity to vary around the mean value, which indeed equals the prescribed velocity. The standard deviation of the error linearly decreases with mesh width, and drops below 1 % for elements sizes below 0.5 km. We therefore recommend using an element size of below 1 km in the ice front vicinity for ice sheet simulations.

Acknowledgements. A. Humbert acknowledges support of the DLR proposal HYD2059 which provides TerraSAR-X data for the project HGF-Alliance Remote Sensing and Earth System Dynamics.

References

- Benn, D. I., Warren, C. R., and Mottram, R. H.: Calving processes and the dynamics of calving glaciers, *Earth-Sci. Rev.*, 82, 143–179, doi:10.1016/j.earscirev.2007.02.002, 2007. 5487
- Brown, C., Meier, M., and Post, A.: Calving speed of Alaska tidewater glaciers, with application to Columbia Glacier, US Geological Survey Professional Paper 1258-C, US Geological Survey, 1982. 5497
- Chang, Y.-C., Hou, T., Merriman, B., and Osher, S.: A level set formulation of Eulerian interface capturing methods for incompressible fluid flows, *J. Comput. Phys.*, 124, 449–464, 1996. 5488
- Courant, R., Friedrichs, K., and Lewy, H.: Über Die Partiellen Differenzgleichungen der Mathematischen Physik, *Math. Ann.*, 100, 32–74, 1928. 5495
- Cuffey, K. M. and Paterson, W. S. B.: *The Physics of Glaciers*, Academic Press, Elsevier, Burlington, Massachusetts, 2010. 5486, 5487, 5491, 5495
- Donea, J. and Huerta, A.: *Finite Element Methods for Flow Problems*, John Wiley & Sons, Chichester, UK, 2003. 5493
- Echelmeyer, K. and Harrison, W. D.: Jakobshavns Isbrae, West Greenland: seasonal variations in velocity – or lack thereof, *J. Glaciol.*, 36, 82–88, 1990. 5488
- Ettema, J., van den Broeke, M. R., van Meijgaard, E., van de Berg, W. J., Bamber, J. L., Box, J. E., and Bales, R. C.: Higher surface mass balance of the Greenland ice

The dynamic response of Jakobshavn Isbræ to calving rate perturbations

J. H. Bondzio et al.

Title Page

Abstract

Introduction

Conclusions

References

Tables

Figures

◀

▶

◀

▶

Back

Close

Full Screen / Esc

Printer-friendly Version

Interactive Discussion

sheet revealed by high-resolution climate modeling, *Geophys. Res. Lett.*, 36, L12501, doi:10.1029/2009GL038110, 2009. 5495

Glen, J. W.: The flow law of ice: a discussion of the assumptions made in glacier theory, their experimental foundations and consequences, *IASH Publ.*, 47, 171–183, 1958. 5490

5 Gogineni, S., Yan, J.-B., Paden, J., Leuschen, C., Li, J., Rodriguez-Morales, F., Braaten, D., Purdon, K., Wang, Z., Liu, W., and Gauch, J.: Bed topography of Jakobshavn Isbræ, Greenland, and Byrd Glacier, Antarctica, *J. Glaciol.*, 60, 813–833, doi:10.3189/2014JoG14J129, 2014. 5488

Greve, R. and Blatter, H.: *Dynamics of Ice Sheets and Glaciers*, Springer, Berlin, Germany, 2009. 5491, 5492

10 Groß, S., Reichelt, V., and Reusken, A.: A finite element based level set method for two-phase incompressible flows, *Comput. Vis. Sci.*, 9, 239–257, doi:10.1007/s00791-006-0024-y, 2006. 5488

Habermann, M., Truffer, M., and Maxwell, D.: Changing basal conditions during the speed-up of Jakobshavn Isbræ, Greenland, *The Cryosphere*, 7, 1679–1692, doi:10.5194/tc-7-1679-2013, 2013. 5489

Howat, I. M., Ahn, Y., Joughin, I., van den Broeke, M. R., Lenaerts, J. T. M., and Smith, B.: Mass balance of Greenland's three largest outlet glaciers, 2000–2010, *Geophys. Res. Lett.*, 38, doi:10.1029/2011GL047565, 2011. 5489, 5500

20 Howat, I. M., Negrete, A., and Smith, B. E.: The Greenland Ice Mapping Project (GIMP) land classification and surface elevation data sets, *The Cryosphere*, 8, 1509–1518, doi:10.5194/tc-8-1509-2014, 2014. 5495

Joughin, I., Abdalati, W., and Fahnestock, M.: Large fluctuations in speed on Greenland's Jakobshavn Isbrae glacier, *Nature*, 432, 608–610, doi:10.1038/nature03130, 2004. 5489

25 Joughin, I., Howat, I. M., Fahnestock, M., Smith, B., Krabill, W., Alley, R. B., Stern, H., and Truffer, M.: Continued evolution of Jakobshavn Isbrae following its rapid speedup, *J. Geophys. Res.*, 113, F04006, doi:10.1029/2008JF001023, 2008. 5489

Joughin, I., Smith, B. E., Howat, I. M., Floricioiu, D., Alley, R. B., Truffer, M., and Fahnestock, M.: Seasonal to decadal scale variations in the surface velocity of Jakobshavn Isbrae, Greenland: observation and model-based analysis, *J. Geophys. Res.*, 117, F02030, doi:10.1029/2011JF002110, 2012. 5489, 5501

30

The dynamic response of Jakobshavn Isbræ to calving rate perturbations

J. H. Bondzio et al.

Title Page

Abstract

Introduction

Conclusions

References

Tables

Figures

◀

▶

◀

▶

Back

Close

Full Screen / Esc

Printer-friendly Version

Interactive Discussion

- Nick, F. M., Vieli, A., Andersen, M. L., Joughin, I., Payne, A., Edwards, T. L., Pattyn, F., and van de Wal, R. S. W.: Future sea-level rise from Greenland's main outlet glaciers in a warming climate, *Nature*, 497, 235–238, doi:10.1038/nature12068, 2013. 5489
- Osher, S. and Sethian, J. A.: Fronts propagating with curvature-dependent speed: algorithms based on Hamilton–Jacobi formulations, *J. Comput. Phys.*, 79, 12–49, doi:10.1016/0021-9991(88)90002-2, 1988. 5487, 5491
- Podrasky, D., Truffer, M., Fahnestock, M., Amundson, J. M., Cassotto, R., and Joughin, I.: Outlet glacier response to forcing over hourly to interannual timescales, *Jakobshavn Isbræ, Greenland, J. Glaciol.*, 58, 1212–1226, doi:10.3189/2012JoG12J065, 2012. 5489
- Pralong, A. and Funk, M.: A level-set method for modeling the evolution of glacier geometry, *J. Glaciol.*, 50, 485–491, doi:10.3189/172756504781829774, 2004. 5488, 5492
- Rignot, E. and Mouginot, J.: Ice flow in Greenland for the International Polar Year 2008–2009, *Geophys. Res. Lett.*, 39, 1–7, doi:10.1029/2012GL051634, 2012. 5488, 5496, 5511
- Rignot, E., Jacobs, S., Mouginot, J., and Scheuchl, B.: Ice-shelf melting around Antarctica, *Science*, 341, 266–270, doi:10.1126/science.1235798, 2013. 5486
- Rosenau, R., Schwalbe, E., Maas, H.-G., Baessler, M., and Dietrich, R.: Grounding line migration and high-resolution calving dynamics of Jakobshavn Isbræ, West Greenland, *J. Geophys. Res.-Earth*, 118, 382–395, doi:10.1029/2012JF002515, 2013. 5489
- Seroussi, H., Morlighem, M., Rignot, E., Larour, E., Aubry, D., Ben Dhia, H., and Kristensen, S. S.: Ice flux divergence anomalies on 79north Glacier, Greenland, *Geophys. Res. Lett.*, 38, L09501, doi:10.1029/2011GL047338, 2011. 5496
- Seroussi, H., Morlighem, M., Larour, E., Rignot, E., and Khazendar, A.: Hydrostatic grounding line parameterization in ice sheet models, *The Cryosphere*, 8, 2075–2087, doi:10.5194/tc-8-2075-2014, 2014. 5490
- Sethian, J.: Evolution, implementation, and application of level set and fast marching methods for advancing fronts, *J. Comput. Phys.*, 169, 503–555, doi:10.1006/jcph.2000.6657, 2001. 5491
- Truffer, M. and Echelmeyer, K. A.: Of isbræ and ice streams, *Ann. Glaciol.*, 36, 66–72, doi:10.3189/172756403781816347, 2003. 5489
- van der Veen, C., Plummer, J. C., and Stearns, L. A.: Controls on the recent speed-up of Jakobshavn Isbræ, West Greenland, *J. Glaciol.*, 57, 770–782, doi:10.3189/002214311797409776, 2011. 5489, 5502

The dynamic response of Jakobshavn Isbræ to calving rate perturbations

J. H. Bondzio et al.

Title Page

Abstract

Introduction

Conclusions

References

Tables

Figures

◀

▶

◀

▶

Back

Close

Full Screen / Esc

Printer-friendly Version

Interactive Discussion



Vieli, A. and Nick, F. M.: Understanding and modelling rapid dynamic changes of tidewater outlet glaciers: issues and implications, *Surv. Geophys.*, 32, 437–458, doi:10.1007/s10712-011-9132-4, 2011. 5487, 5489, 5501

Winkelmann, R., Martin, M. A., Haseloff, M., Albrecht, T., Bueller, E., Khroulev, C., and Levermann, A.: The Potsdam Parallel Ice Sheet Model (PISM-PIK) – Part 1: Model description, *The Cryosphere*, 5, 715–726, doi:10.5194/tc-5-715-2011, 2011. 5487

Zwally, H. J., Jun, L., Brenner, A. C., Beckley, M., Cornejo, H. G., Dimarzio, J., Giovinetto, M. B., Neumann, T. A., Robbins, J., Saba, J. L., Donghui, Y., and Wang, W.: Greenland ice sheet mass balance: distribution of increased mass loss with climate warming; 2003–07 versus 1992–2002, *J. Glaciol.*, 57, 88–102, doi:10.3189/002214311795306682, 2011. 5488, 5495

Table A1. Symbols and model parameters.

Symbol	Quantity
μ	Ice viscosity
B	Ice viscosity parameter
$\dot{\epsilon}_e$	Effective strain rate
n	Glen's flow law parameter
α	Basal friction parameter
N	Effective basal pressure
\mathbf{v}	Depth-averaged ice velocity
H	Ice thickness
a_s	Surface mass balance
a_b	Basal mass balance
Ω	Computational domain
Ω_i	Ice domain
Ω_i^h	Numerical ice domain
Ω_c	Ice free domain
Γ	Ice boundary
Γ^h	Numerical ice boundary
φ	Level-Set Function
\mathbf{n}	Unit surface normal on Γ
\mathbf{w}	Ice front velocity
\mathbf{a}	Ablation velocity
a^\perp	Ablation rate
\mathbf{c}	Calving velocity
c^\perp	Calving rate
s	Scaling function
p	Perturbation function
Δt	Perturbation duration
p_0	Perturbation strength
L	Seasonal calving period length
ϕ_0	Phase shift
P	Perturbation measure
Q_{cf}	Calving flux

The dynamic response of Jakobshavn Isbræ to calving rate perturbations

J. H. Bondzio et al.

Title Page

Abstract Introduction

Conclusions References

Tables Figures

◀ ▶

◀ ▶

Back Close

Full Screen / Esc

Printer-friendly Version

Interactive Discussion



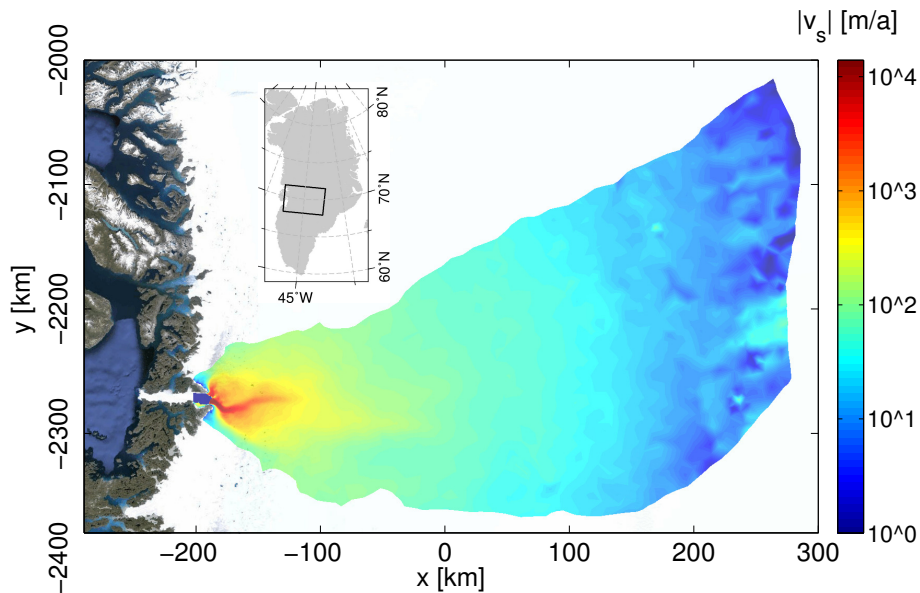


Figure 1. Observed ice surface velocities 2008/2009 (Rignot and Mouginot, 2012) of the Jakobshavn Isbræ drainage basin used for modelling (logarithmic scale). Background image from Google Earth®.

The dynamic response of Jakobshavn Isbræ to calving rate perturbations

J. H. Bondzio et al.

Title Page	
Abstract	Introduction
Conclusions	References
Tables	Figures
◀	▶
◀	▶
Back	Close
Full Screen / Esc	
Printer-friendly Version	
Interactive Discussion	



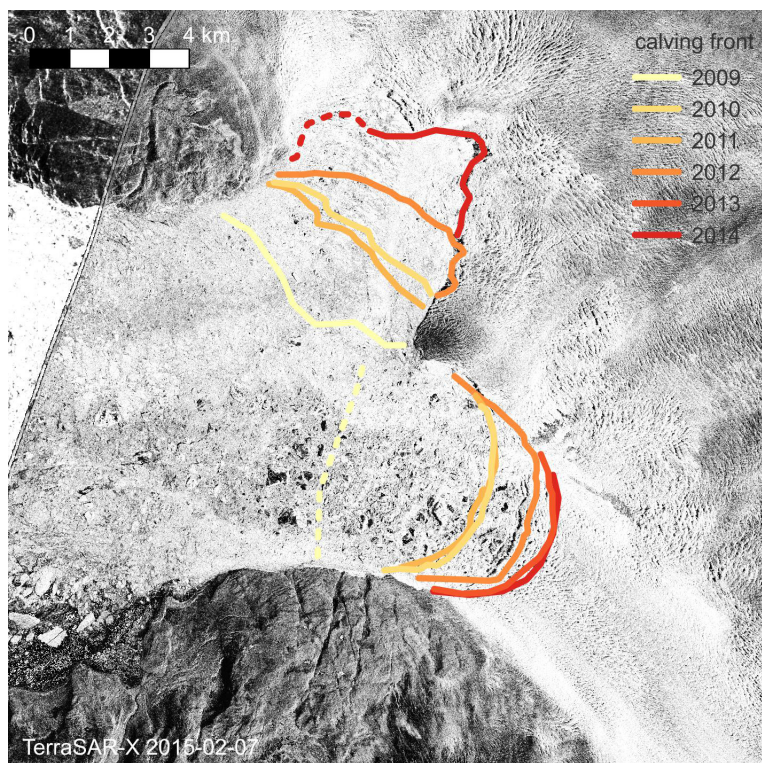


Figure 2. Winter (February–March) ice front positions from 2009 to 2014 superimposed on a TerraSAR-X scene from 7 February 2015 (©DLR). Striped lines are used in case of ambiguous ice front positions.

The dynamic response of Jakobshavn Isbræ to calving rate perturbations

J. H. Bondzio et al.

Title Page	
Abstract	Introduction
Conclusions	References
Tables	Figures
◀	▶
◀	▶
Back	Close
Full Screen / Esc	
Printer-friendly Version	
Interactive Discussion	



The dynamic response of Jakobshavn Isbræ to calving rate perturbations

J. H. Bondzio et al.

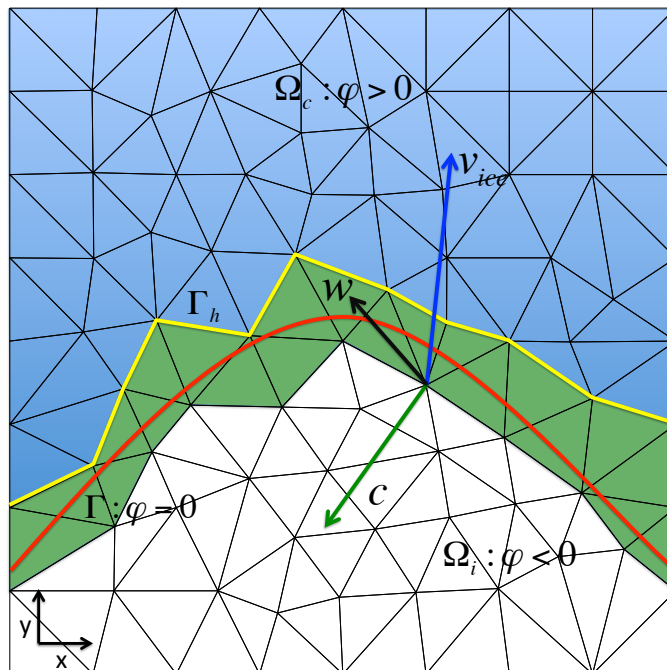


Figure 3. Schematic of the ice margin. The red line marks the zero level-set, the yellow one the numerical ice front. Blue triangles are ice-free elements, white ones the ice-filled ones and green ones the front elements. The three vectors show an example of the evaluation of the boundary velocity \mathbf{w} at a finite element node.

Title Page

Abstract

Introduction

Conclusions

References

Tables

Figures

◀

▶

◀

▶

Back

Close

Full Screen / Esc

Printer-friendly Version

Interactive Discussion



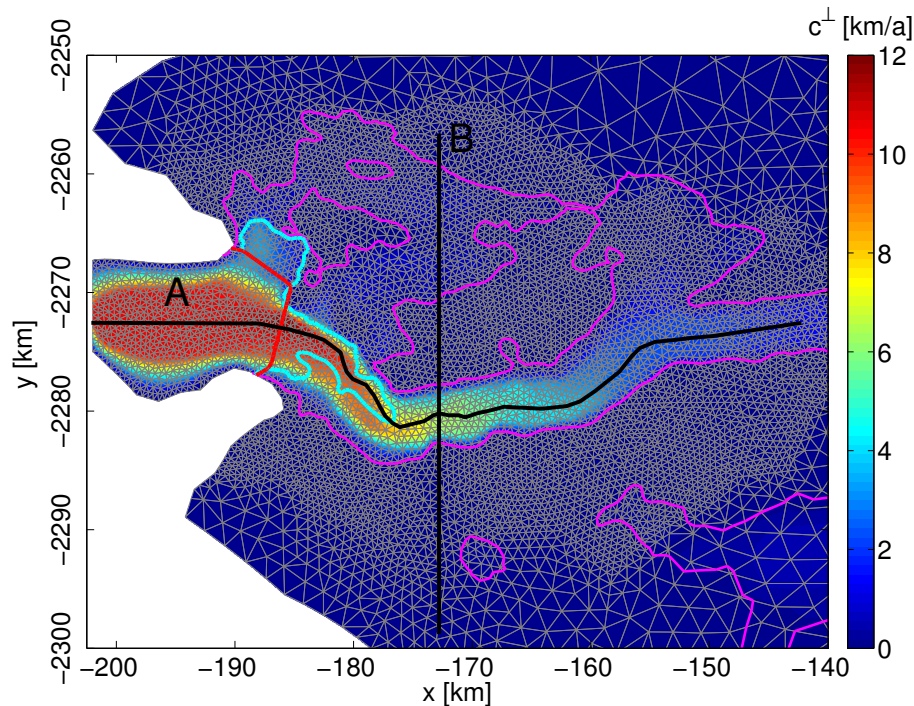


Figure 4. The applied calving rate field c_0^\perp in the region of fast flow, which has been derived from modelled ice velocities at the end of the geometry relaxation run. The red line indicates the zero level-set of the initial LSF used for geometry relaxation and as start position for the ice front during the experiments. The turquoise line marks the grounding line. Purple contours indicate zero bedrock elevation. Black lines are the tracks “along-trough” (A) and “across-trough” (B) used in Fig. 6. The start points of tracks A and B are the western and northern end, respectively. The finite element mesh is displayed in grey.

The dynamic response of Jakobshavn Isbræ to calving rate perturbations

J. H. Bondzio et al.

Title Page	
Abstract	Introduction
Conclusions	References
Tables	Figures
◀	▶
◀	▶
Back	Close
Full Screen / Esc	
Printer-friendly Version	
Interactive Discussion	



The dynamic response of Jakobshavn Isbræ to calving rate perturbations

J. H. Bondzio et al.

Title Page

Abstract

Introduction

Conclusions

References

Tables

Figures

◀

▶

◀

▶

Back

Close

Full Screen / Esc

Printer-friendly Version

Interactive Discussion

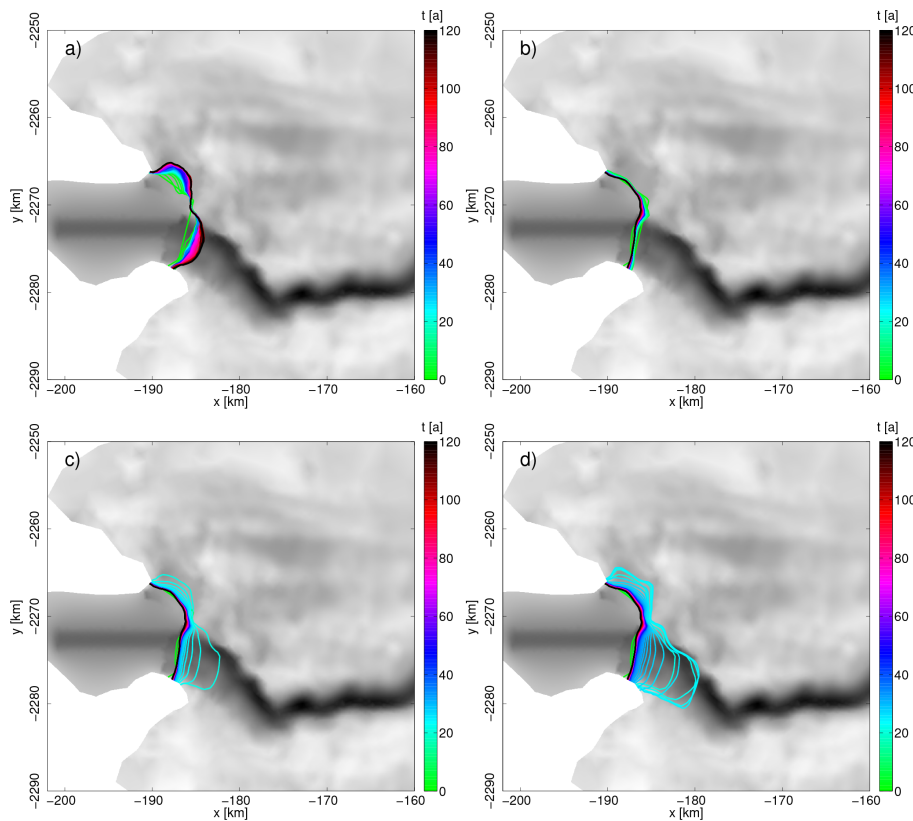


Figure 5. Ice front position for experiments A, B1, B2 and C4 at the start of each year, plotted over basal topography (grey).

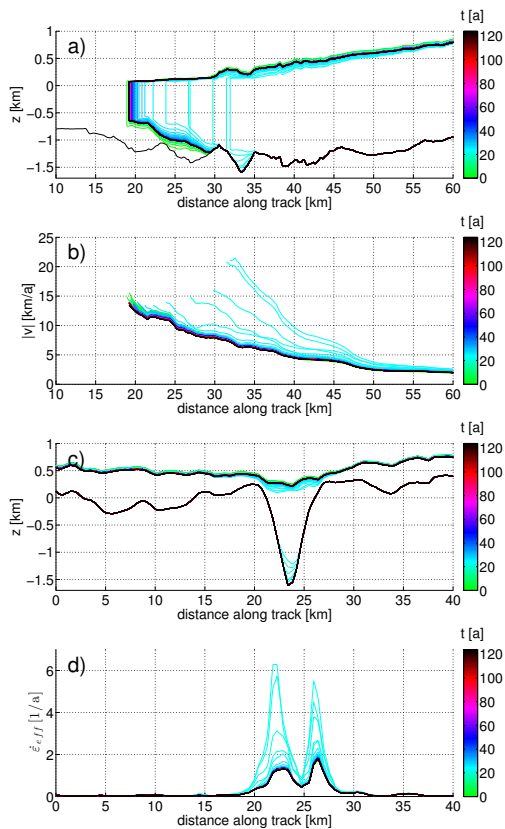


Figure 6. Section values of experiment C4. **(a)** ice geometry and **(b)** ice velocity along-trough. **(c)** Ice geometry and **(d)** effective strain rates across-trough. Positions of the tracks are given in Fig. 4.

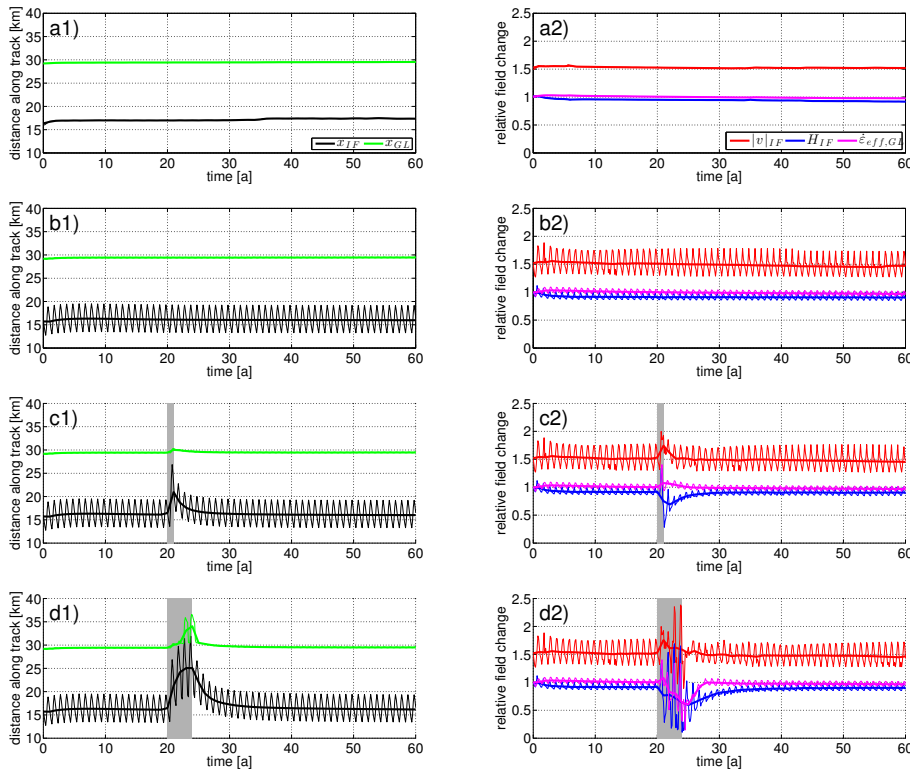


Figure 7. Ice front and grounding line position along-trough (left column), as well as values of ice front thickness, ice velocity and effective strain rate relative to their initial value along-trough (right column) over time for experiments (a) A, (b) B1, (c) B2 and (d) C4. Perturbation intervals are marked in grey. Relative values for ice velocity have been shifted up by 0.5 for better visibility.

The dynamic response of Jakobshavn Isbræ to calving rate perturbations

J. H. Bondzio et al.

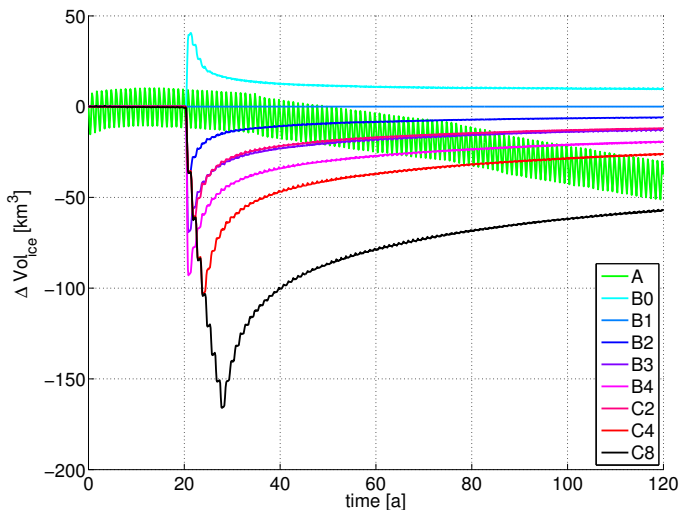


Figure 8. Difference in total ice volume of the different simulations to experiment B1 over time. The smooth ice volume profile of experiment A causes its difference to experiment B1 to oscillate.

[Title Page](#)[Abstract](#)[Introduction](#)[Conclusions](#)[References](#)[Tables](#)[Figures](#)[◀](#)[▶](#)[◀](#)[▶](#)[Back](#)[Close](#)[Full Screen / Esc](#)[Printer-friendly Version](#)[Interactive Discussion](#)

The dynamic response of Jakobshavn Isbræ to calving rate perturbations

J. H. Bondzio et al.

Title Page

Abstract

Introduction

Conclusions

References

Tables

Figures

◀

▶

◀

▶

Back

Close

Full Screen / Esc

Printer-friendly Version

Interactive Discussion

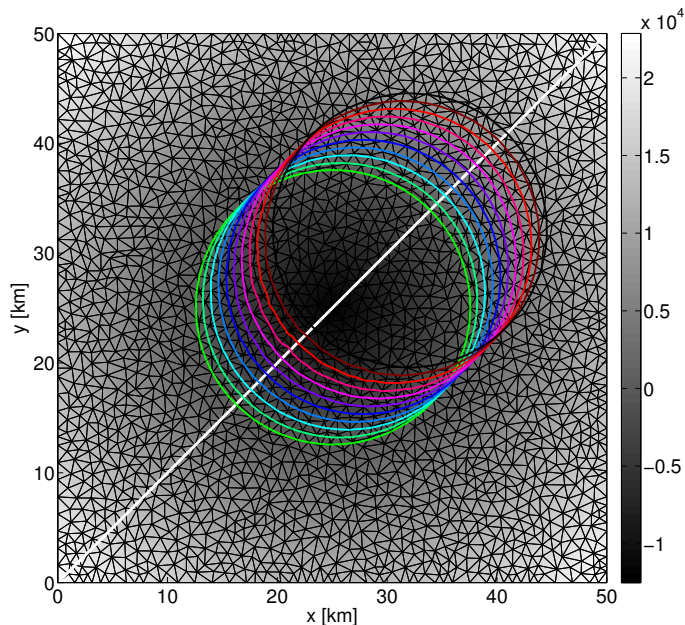


Figure A1. 0-level-set position at the start of every year, plotted over φ_0 , which is shaded in grey. An example of the mesh with element size 1 km is marked in black. The white diagonal marks the straight along which the velocity of the 0-level-set is tracked.

The dynamic response of Jakobshavn Isbræ to calving rate perturbations

J. H. Bondzio et al.

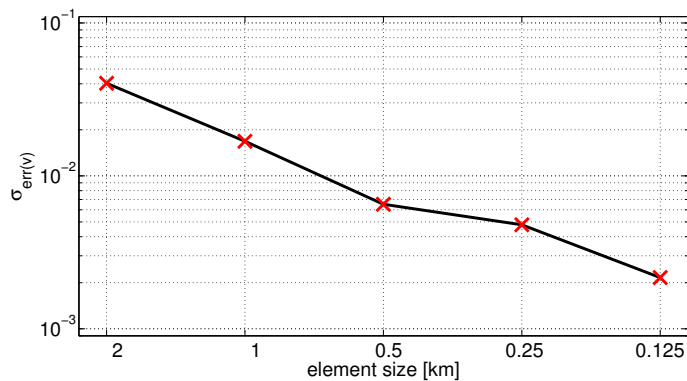


Figure A2. Standard deviation of the relative numerical error in advection velocity of the 0-level-set depending on mesh element size.

[Title Page](#)[Abstract](#)[Introduction](#)[Conclusions](#)[References](#)[Tables](#)[Figures](#)[◀](#)[▶](#)[◀](#)[▶](#)[Back](#)[Close](#)[Full Screen / Esc](#)[Printer-friendly Version](#)[Interactive Discussion](#)